Circular Polarized Antennas With Harmonic Radar: Passive Nonlinear Tag Localization

Vishal G Yadav, *Graduate Student Member, IEEE*, Leya Zeng, *Graduate Student Member, IEEE*, and Changzhi Li, *Senior Member, IEEE*

***Abstract*—This research proposes a high performance, low-profile planar design, and demonstration of circularly polarized harmonic antenna arrays for 4 and 8 GHz harmonic radar system, which is equipped, and the antenna's circular polarization (CP) performance is tested using a passive nonlinear harmonic tag (snowflake) in a noisy environment. This work mainly concentrates on investigation of the wave polarization (circular), gain estimation and impedance matching of the antenna arrays that will be potentially assembled to the second-order harmonic radar system operating at 4 and 8 GHz, which plays a critical role in 2-D tag localization and post processing methods. The passive snowflake tag design is implemented in the simulation to determine the current distribution and gain plot patterns in comparison to a classic dipole antenna tag structure. In experiments: a combination of fundamental circular polarized (left-hand) antennas were demonstrated to find axial ratio $\leq$ 3 dB band. A novel tag 2-D localization measurement, combination of CP harmonic antenna arrays is utilized to perform and obtain the circular polarized received signal power in dBm versus angle rotation by every 10° on a rotating platform setup. Finally, the wireless tag tracking result is achieved by using the designed circularly polarized antennas and the passive nonlinear tag orientation setup.**

***Index Terms*—Antenna array, axial ratio (A.R.), circular polarization (CP), gain estimation, harmonic radar, impedance matching, linear polarization (LP), snowflake passive tag, tag localization process.**

I. Introduction

WIRELESS signal technology industry has encountered considerable challenges in maintaining consistent electromagnetic (EM) waves across a certain distance using conventional fundamental tone radar system for tracking applications. Considering a second-order harmonic radar system with the ability to generate a strong signal, it becomes effective in detecting radio frequency identification (RFID) passive tags that are nonlinear and affixed or integrated into specific items, creatures, such as insects, amphibians, and invertebrates. This technology serves the purpose of tracking the location and observing the movements of these entities, monitoring their behavioral patterns and characteristics in the presence of other surrounding objects discussed in [1], [2], [3], [4], [5], [6], [18], [35], and [38].

To enhance the tag localization technology, it is equally necessary to implicate a stable continuous reflected signal power throughout the process discussed in [24]. The type of transmitter (Tx) and receiver (Rx) antennas and its wave propagation orientation [linear polarization (LP)/CP] will depend mainly on the radar architecture, operation of frequency range, nonlinear passive tag design, far-field region spaced from the radar antennas to the tag. Examples of different antenna types, such as horn antenna, dielectric lens antenna, slotted waveguide antenna, and microstrip patch antenna, and their wave propagation are discussed in [5], [6], [7], [8], and [30], which will result in obtaining a stable reflected signal from the transponders. Most of these antenna types discussed above are based on LP wave patterns.

In order to accurately model and satisfy these key specification requirements for a second-order harmonic radar for snowflake passive tag 2-D localization, this article proposes and utilizes 50 Ω microstrip corporate-fed planar patch antenna array comprising of four-antenna elements for harmonic frequencies. Tx antenna operates at (4 GHz) designed on an FR-4 substrate ($\varepsilon_0 = 4.3$; $\alpha = 0.02$) for the generation of the fundamental tone. The Rx antenna will operate in the second-order harmonic frequency (8 GHz) designed on a Rogers 3003 ($\varepsilon_0 = 3.0$; $\alpha = 0.0015$). Based on the electric field vector's rotation direction, circular polarized radar antenna arrays are categorized into: right-hand circular polarization (RHCP) and left-hand circular polarization (LHCP).

RHCP antenna array is formed when the electric field vector rotates in a clockwise (CW) direction, while LHCP antenna array is created when it rotates in a counterclockwise (CCW) direction at a point in the far-field. In an ideal scenario, both LHCP and RHCP antenna arrays will generate identical circular polarized wave propagation in the distant radiating region. To achieve CP, the LHCP array is designed by truncated corner cut method. This method is considered the most efficient, feasible, cost-effective, and easy to implement to the harmonic radar system. The designed fundamental antenna pairs are initially designed, simulated in AWR microwave office, an antenna analysis, and then it is replicated in Ansys HFSS. It is finally validated by performing impedance matching testing, two-antenna gain approximation

Manuscript received 30 September 2023; revised 24 January 2024; accepted 11 March 2024. Date of publication 18 March 2024; date of current version 24 April 2024. This work was supported in part by National Science Foundation (NSF) under Grant ECCS-2030094 and in part by Ballocator LLC. Recommended by Lead Guest Editor Pai-Yen Chen and Guest Editor Chung-Tse Michael Wu. *(Corresponding authors: Leya Zeng; Changzhi Li.)*

The authors are with the Department of Electrical and Computer Engineering, Texas Tech University, Lubbock, TX 79409 USA (e-mail: visyadav@ttu.edu; lezeng@ttu.edu; changzhi.li@ttu.edu).

Digital Object Identifier 10.1109/JSAS.2024.3378157

method, and polarization tests in the far-field radiating region spaced at 1.80 m. The circular wave propagation pattern for E_X, E_Y magnitude plots in the $X-Y$ coordinate plane and axial ratio (A.R.) measured as 0.85 dB for 4 GHz LHCP array and 0.77 dB for 8 GHz LHCP array, which is ≤ 3 dB A.R. bandwidth. The A.R. measures an antenna's polarization purity, which is a crucial factor in distinguishing an LP array from a CP array. A higher A.R. value is associated with the LP array, indicating a less pure polarization state. On the other hand, the CP array exhibits an A.R. below 3 dB, signifying a superior polarization state compared to the linear polarized antenna array.

For novelty work, the tag tracking and 2-D localization behavior for the snowflake antenna tag is characterized with the designed and validated circular polarized harmonic Tx and Rx antennas in the far-field region at a distance of 0.40 m. The second-order reflected received power in dBm versus angle rotation in degrees is plotted to verify that the signal power is constant and stable in the far-field region even with the rotation of the Tx antenna by keeping the Rx antenna and the passive tag in stationary positions. Tx circular polarized antenna radiates the fundamental tone at 4 GHz, and it is rotated every 10° up to 360° on a polarization rotating setup. This circular polarized wave is incident on the snowflake tag. Since the tag exists, it generates a harmonic wave of 8 GHz, which is received by the Rx harmonic circular polarized antenna. The received signal is a constant stable signal with less signal fluctuation, which carries the target information for further processing.

The rest of this article is organized as follows. Section II includes the generic second-order harmonic radar system and its fundamental theory of each block. Section III discusses the difference in snowflake tag implementation and classical diode simulation and plots. Section IV discusses the design, simulation and experimental validation of 4 and 8 GHz LHCP antennas. Section V depicts the tag localization test combination with the LHCP radar antennas with the passive snowflake tag. Finally, this article is concluded in Section VI.

II. Second-Order Harmonic Radar System

A. Harmonic Frequency Theory

A nonlinear radar that produces harmonics of higher order is often termed as a harmonic radar architecture. In the wave and propagation theory, the term "harmonic frequency" is simply referred to as a harmonic, which is an integer multiple of a fundamental single tone. The harmonic frequencies are the higher order tones of the original base frequency represented in mathematical form as

$$f_n = n \times f_0 \tag{1}$$

where f_n denotes harmonic frequency, "n" denotes a positive integer such as (1, 2, 3 …n^{th}) harmonic term and f_0 denotes fundamental frequency of first-order tone discussed in [9], [23]. Harmonic radars are typically operated by radiating harmonic frequencies generated by objects in the response to the incident transmitted signal using a second-order harmonic radar discussed in [19], [20], [21], [22], and [26] using LP antennas. Generic harmonic radar operating at Tx: 4 GHz and Rx: 8 GHz frequency, which is easily implemented to the functioning LP/CP harmonic antennas shown in Fig. 1. Overall tag tracking application using nonlinear harmonic radar system is displayed.

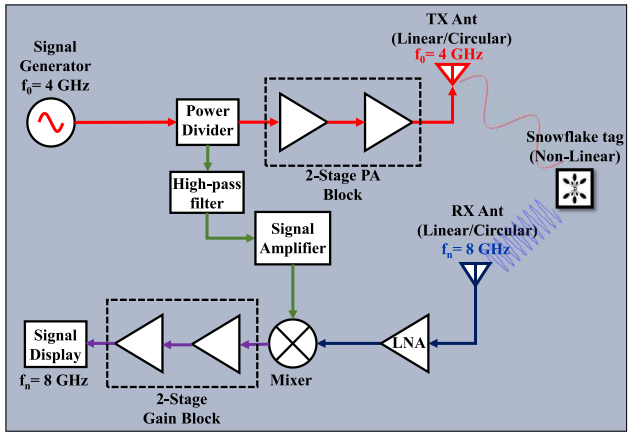

Fig. 1. Generic block diagram for second order harmonic system.

B. Tx Block

The Tx component generates a 4 GHz fundamental frequency from the signal generator. This generated signal is then sent to the power divider circuit and is further divided into two equal fundamental subsignals, which is either a Wilkinson power divider or a power splitter. One of these subsignals is transmitted to the two-stage power amplifier block and measured in dBm. This amplifier block is crucial in improving the signal strength, linearity, and bandwidth for a wide range of frequencies. This amplified subsignal is incident from the fundamental transmitting antenna designed at 4 GHz frequency toward the nonlinear passive tag

$$T_x(t) = \cos(\omega t + \phi) \tag{2}$$

$$\omega_1(t) = 2\pi f_0. \tag{3}$$

In this context, $T_x(t)$ denotes the signal being transmitted at a specific time (t), ϕ symbolizes the phase constant, and ω_1 signifies the angular frequency in radians per second, encompassing the base frequency $f_0 = 4$ GHz.

C. Frequency Doubler Block

The other fundamental subsignal passes through a high-pass filter, wherein only higher frequency bands will pass through it. These higher frequency signals will undergo a signal amplification module that is additionally responsible for enhancing the power gain of the second-order tone. Subsequently, this harmonic tone is directed to the local oscillator input port of the mixer module. The second-order harmonic frequency signal is written as

$$X(t) = \cos(2(\omega t) + \phi) \tag{4}$$

$$\omega_2(t) = 2(2\pi f_0) \tag{5}$$

$$\omega_2(t) = 4\pi f_0. \tag{6}$$

Here, $4\pi f_0$ indicates the frequency multiplication factor for generating the second-order tone.

D. Rx Chain Block

The Rx module comprises the designed (LP/CP) antenna, which captures the reflected harmonic signal sent by the snowflake nonlinear tag. This captured weak reflected second-order tone is then subjected to signal amplification as it passes through a low-noise amplifier. Subsequently, it is directed to the RF input port of a mixer module designed to handle higher frequency inputs. The mixer unit combines the second-order multiplied local oscillator (LO) input signal with the RF harmonic input signal to produce an intermediate frequency (IF) output of similar harmonic frequency discussed in [27]. The IF output signal is then directed to a two-stage operational amplifier gain unit to further amplify the second-order harmonic signal. This amplified signal is displayed on a spectrum display for result analysis. The signal received from the tag is recorded as follows:

$$R_x(t) = \cos\left(4\pi f_0 t - \frac{4\pi d}{\lambda} - \Delta\phi(t)\right) \tag{7}$$

where d stands for the distance between the radar antennas and the snowflake tag, λ denotes for the $2f_0$, and $\Delta\phi(t)$ is the residual phase shift from the nonlinear tag.

III. Antenna Tag Simulation

A. Dipole Tag Simulation

The classical dipole antenna is $\lambda/2$ length, which is symmetrical to the arm elements connected by a nonlinear component at the center of the dipole as discussed in [2]. The nonlinear component used in the tag design primarily consists of a Schottky diode, that is situated at the center-feed of the antenna tag that is helpful in the rectification mechanism of the tag's nonlinearity discussed in [10], [19], [34], [38], and [39]. When a fundamental frequency at "f_1" from the transmitting antenna is transmitted to the Schottky diode, it picks-up this signal that biases the diode as a voltage source at "V_1" and harmonic current amplitudes at "$I_1,\ I_2,\ I_3,\ I_4, \ldots$" are generated by the diode. The diode resistance at f_1 is represented as $R_1 = V_1/I_1$. This reflected signal from the diode consists of higher integer multiples of harmonic frequencies, particularly reflecting the second-order harmonic at "f_2" has a harmonic current as I_2 and all the other higher order harmonics are neglected. This second-order harmonic frequency is received by the receiving antenna for further signal analysis.

Several studies on the dipole antenna tag design were conducted based on arm shape, dielectric substrate material, dipole length to match the impedance, lesser tag weight to increase the efficiency of the tag performance and peak-amplitude versus angle as discussed in [11], [12], and [25].

This work presents the implementation of dipole tag with dc short by performing sanity simulation check if the tag could be used for harmonic design frequencies. To ensure that it is equipped for reflecting a stable return signal power, the Tx CP antenna is rotated for tag tracking purposes. This design approach discusses $L = \lambda/4$ length dipole antenna with dc short connecting the symmetrical dipole elements, which is primarily considered as a nonlinear harmonic tag. Schottky diode terminals connecting the symmetrical arms were implemented as differential ports P_1 and P_2 to match the diode impedance with the load impedance of antenna elements as shown in Fig. 2. This diode does not require any external power supply connected to the dipole tag. This tag is simulated at multiple frequencies at 4 and 8 GHz to analyze dipole tag performance to harmonic frequencies.

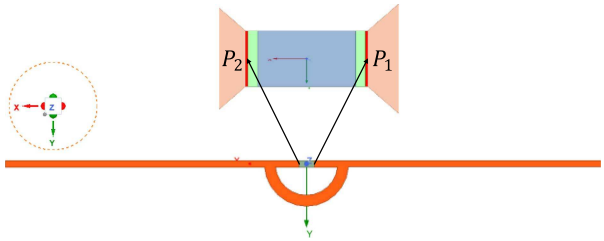

Fig. 2. Classic dipole antenna with dc short and differential ports.

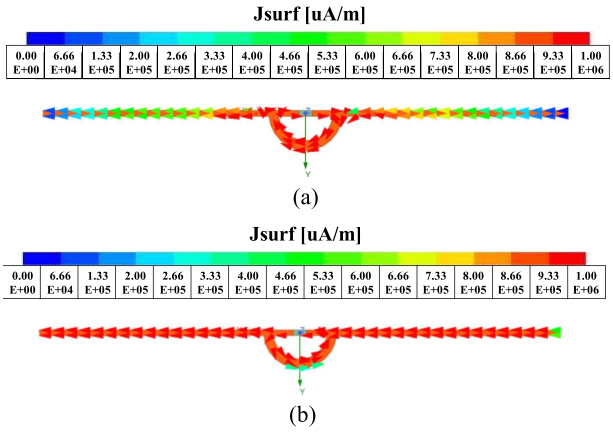

Fig. 3. Current distribution vectors for dipole antenna tag. (a) 4 GHz. (b) 8 GHz.

Fig. 3(a) and (b) depicts the uniform current distribution plots for fundamental and harmonic tones, which help us to understand the propagation of EM waves through the elements. In Fig. 3(b), current vectors of greater magnitude are maximum when compared with the current vectors in Fig. 3(a). Since the current flow is higher for the second-harmonic tone, the gain plot in Fig. 4. shows 3.00 dB gain for 8 GHz in comparison with 1.73 dB gain for 4 GHz frequency. This indicates that the reflected harmonic signal power from the dipole tag is higher to the incident transmitted signal power.

B. Snowflake Tag Simulation

A novel design of a non-linear harmonic tag (snowflake) was introduced in [34] and is based on the dipole configuration. This design further improved the tag's signal-to-noise ratio by four times compared with the conventional dipole configuration. The tag's base design, shown in Fig. 5, is simulated in

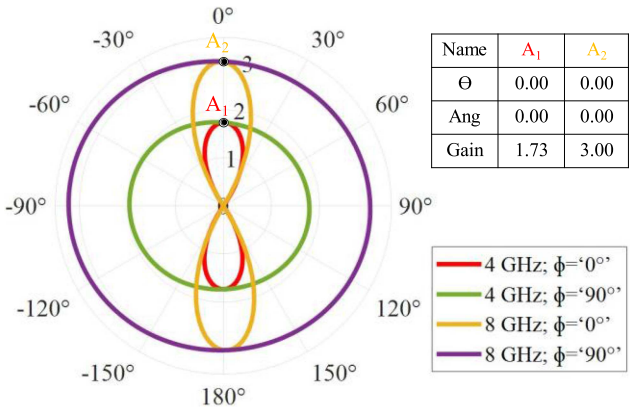

Name	A_1	A_2
Θ	0.00	0.00
Ang	0.00	0.00
Gain	1.73	3.00

Fig. 4. 2-D simulation gain in dB plots for dipole antenna tag: 4 and 8 GHz.

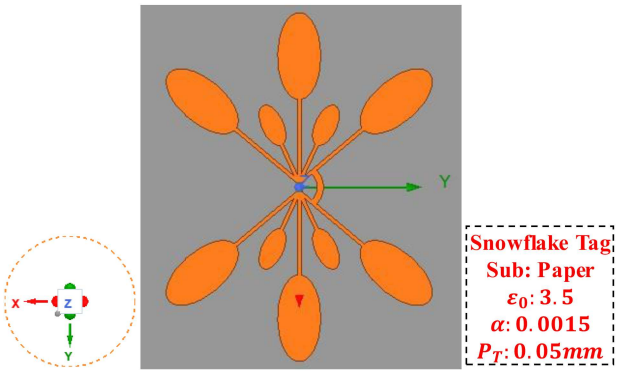

Fig. 5. Snowflake antenna tag with DC short with differential ports implementation.

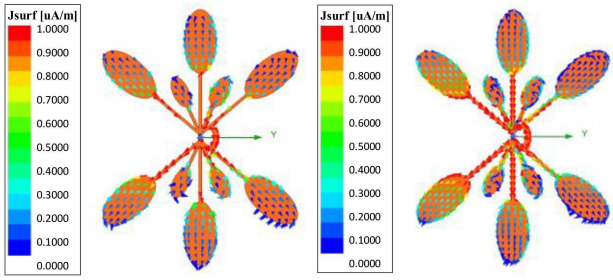

Fig. 6. Current distribution vectors for snowflake antenna tag: (a) 4 GHz; (b) 8 GHz.

HFSS to observe its current flow and gain formation, shown in Figs. 6 and 7. The tag design is simulated on a paper substrate ($\varepsilon_0 = 3.5;\ \alpha = 0.0015$) indicated in gray color consisting of a paper thickness of ($P_T = 0.05$ mm).

The snowflake tag performance is characterized by the second-order conversion efficiency "η" represented in (8). It primarily equals to the ratio of the maximum output harmonic power $(P_H)_{\max}$ radiated by the tag to the input fundamental power (P_F) incident to the tag. The second-order harmonic

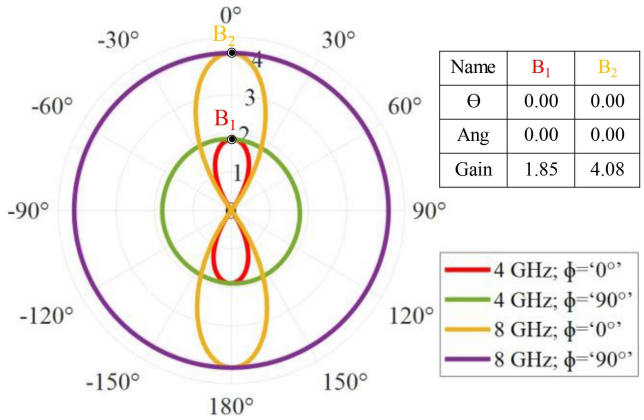

Name	B_1	B_2
Θ	0.00	0.00
Ang	0.00	0.00
Gain	1.85	4.08

Fig. 7. 2-D simulation gain in dB plots for snowflake antenna tag: 4 and 8 GHz.

conversion loss mainly depends on the consideration of the Friis transmission loss equation presented in [33] and [38]

$$\eta = \frac{(P_H)_{\max}}{P_F} \times 100 \tag{8}$$

$$(P_H)_{\max} = \frac{P_F \times G_{Tx} \times G_{Rx} \times \lambda^2}{(4 \times \pi \times R)^2} \tag{9}$$

where G_{Tx} and G_{Rx} stands for the Gains of the fundamental transmitting and the second-order harmonic receiving antennas respectively. λ presents the wavelength of the transmitting antenna and R denoted the distance of separation between the Tx and Rx antennas. The performance of the snowflake tag can be estimated as: 1) when in close proximity with the harmonic antennas, the received harmonic signal conforms to an inverse fourth-power path loss principal concerning both distance of separation and the frequency of operation; 2) when separated at maximum distance the signal power decays quickly.

This new design implementation is expected to perform better than the ideal dipole tag with increased gain improvement and current vectors distribution. The current distribution vector $(Jsurf)$ in μA/m and 2-D Gain plot for harmonic frequencies are shown in Figs. 6(a) and (b), and 7, respectively. Fig. 6(b) indicates that the current vectors of greater magnitude are maximum when compared with the current vectors in Fig. 6(a). The Gain plot for the snowflake tag for both 4 GHz is 1.85 dB and 8 GHz are 4.08 dB which are significantly improved in comparison to the initial dipole tag design discussed in Section III-A. This improved performance helps in enhancing the efficiency of the tag tracking application.

IV. Circular Polarized Harmonic Radar Antennas

A. CP Antenna Array Design Considerations

The ideal LP antenna array is sensitive and propagates an electric field vector that traces a straight line in the far-field radiating boundary. Depending on orientation (vertical or horizontal) position of Tx and Rx antennas facing the snowflake tag only one electric field component is present. If either of the

antennas are misaligned facing the antenna tag, it would result in polarization mismatch and lead to signal loss.

For achieving tag tracking application, a stable continuous circular polarized signal must be utilized that propagates an electric field vector and traces a circular wave pattern with equal (radius) magnitudes in the direction of signal propagation. CP signals are achieved by generating two orthogonal modes having a time-phase difference of 90°. CP is less prone to signal degradation, caused due to the rotation of the Tx and Rx antennas or the tag. Hence, CP signals can still be obtained with minimal signal loss making them an ideal approach when the antenna rotation is relative among each other. There are different methods to excite orthogonal modes, such as single-feed slotted square patch, truncated corners patch coaxial-feed, single truncated corner patch with inset feed, circular patch with unequal X-slit, microstrip feed stacked patch configuration and sequential rotation technique with four-elements truncated subarray, as discussed in [13], [14], [15], [16], [17], [29], respectively.

Based on the current work, to achieve CP signal, it is considered to ensure that the antenna array must be efficient in terms of A.R. in dB, impedance matching S_{11} return loss in dB at the design frequency, higher gain in dB, and wave polarization pattern, which is responsible for the rotation orientation of electric field vectors in the far-field region. All these fundamental antenna design parameters discussed in [32] and [33], are utilized to design, simulate, and validate 4 and 8 GHz CP antenna arrays discussed in [37]. The antenna arrays were designed for LHCP type: LHCP signifies the EM wave rotates in CCW direction to navigate the non-linear tag. Generally, the electric field vector $\vec{E}$ of the Tx CP antenna/Rx CP antenna in the far-field radiation region can be expressed as

$$\vec{E} = E_R\widehat{a_R} + E_L\widehat{a_L} \tag{10}$$

$$E_R = \frac{E_\theta}{\sqrt{2}} - \frac{E_\varphi}{j\sqrt{2}}$$

$$E_L = \frac{E_\theta}{\sqrt{2}} + \frac{E_\varphi}{j\sqrt{2}} \tag{11}$$

$$\widehat{a_R} = \frac{\widehat{a_\theta} - j\widehat{a_\varphi}}{\sqrt{2}}$$

$$\widehat{a_L} = \frac{\widehat{a_\theta} + j\widehat{a_\varphi}}{\sqrt{2}} \tag{12}$$

where E_R depicts the magnitude of electric field vector in CW direction, $\widehat{a_R}$ represents the phase component of the RHCP wave, E_L shows the magnitude of electric field vector in CCW direction, and $\widehat{a_L}$ represents the phase component of the LHCP wave. $|E_R|$=$|E_L|$ and $\angle E_\theta$ *and* $\angle E_\varphi$ must have a phase difference of $\pm 90°$ apart discussed in [32]. The A.R. in linear scale and logarithmic scale can be expressed as follows:

$$\text{A.R.} = \frac{|E_R| + |E_L|}{|E_R| - |E_L|} \tag{13}$$

$$\text{A.R.}_{dB} = 20\log_{10}|\text{A.R.}|\,. \tag{14}$$

For the RHCP wave, the A.R. $= +1$ (linear) and for the LHCP wave, the A.R. $= -1$ (linear). The A.R. bandwidth for a CP antenna is $0 \leq \text{A.R.}_{dB} \leq 3$ dB. In the ideal world, the polarization loss factor (PF) for a CP antenna for desired frequency is 0, i.e., (PF $= 0$).

B. Tx Antenna: 4 GHz CP Antenna Array

The Tx antenna is a CP four-element array designed along the $X-Y$ plane for 4 GHz operating frequency for a LHCP array by incorporating microstrip transmission feedline as discussed in [31], with 50 Ω input port impedance. The array is planar in structure radiating in the Z coordinate plane.

LHCP array was designed based on corporate feed network on an FR-four substrate ($\varepsilon_0 = 4.3$; $\alpha = 0.02$; $Cu_T = 0.035$ mm) with size dimensions of $160 \times 144 \times 1.6$ mm^3.The fabricated array with truncated corner ($\Delta L = 3.48$ mm) elements is designed to form a LHCP array as shown in Fig. 8(a) with other specified key dimension markings. The standard 4 GHz LP array was based on inset fed ($X_0 = 5.1$ mm; $W_0 = 1.45$ mm) design as represented in Fig. 8(b). The array spacing (S_X along x-axis and S_Y along y-axis) is maintained from $\lambda/2 < S$ in mm $< \lambda$.Quarter-wave transformers were added to each element feeding edge for matching the load impedances ($Z_L = 176\,\Omega$) with the input source impedance ($Z_S = 50\,\Omega$) in order to achieve a broadband CP. SubMiniature version A (SMA) connectors in brass metal coating are located at the central-left and central-right of Fig. 8(a) and (b) were soldered to power-in the antenna arrays. The single-feed antenna array is developed by utilizing equal power distribution in [8] throughout all the four-elements with minimum insertion loss and maximum signal transmission through the microstrip transmission lines to reach the antenna elements. The three-equal power split method was initially designed in AWR microwave design environment to determine the magnitude and phase data on Smith chart. The SMA connector feeds the transmission line with a two-way power division through a first $\lambda/4$ wave transformer, which will further divide the power and feeds the upper half-array and the lower half-array elements.

The upper half array and the lower half array are parallelly connected that will undergo into another equal power division through the second and third $\lambda/4$ wave transformers, respectively. At the junction of each $\lambda/4$ wave transformers, the widths of the microstrip feedline will reduce based on impedance matching design calculations.

The simulation and optimization results were performed to achieve the fundamental parameters: impedance matching S_{11} in dB in Fig. 9, 2-D gain plot in Fig. 10, A.R. versus frequency plot in Fig. 11(c), and the measurement of the angle versus received power signal is plotted in Fig. 11(a). The A.R. simulation data points in Fig. 11(c) were further verified by extracting the simulated electric field vectors of $|E_x|$ and $|E_y|$ along x- and y-axes, respectively. The phase angles $\angle E_x$ and $\angle E_y$ along the $\angle\Theta = 0°$ and $\angle\phi = 0°$ were also simulated to understand the polarization orientation emitting a circular wave pattern in the far-field radiating region in the z-axis radiation boundary. 4 GHz LHCP Tx array is designed to radiate fundamental tone for snowflake tag tracking application. The performance of the antenna array is experimented with LP array in Fig. 8(b) to

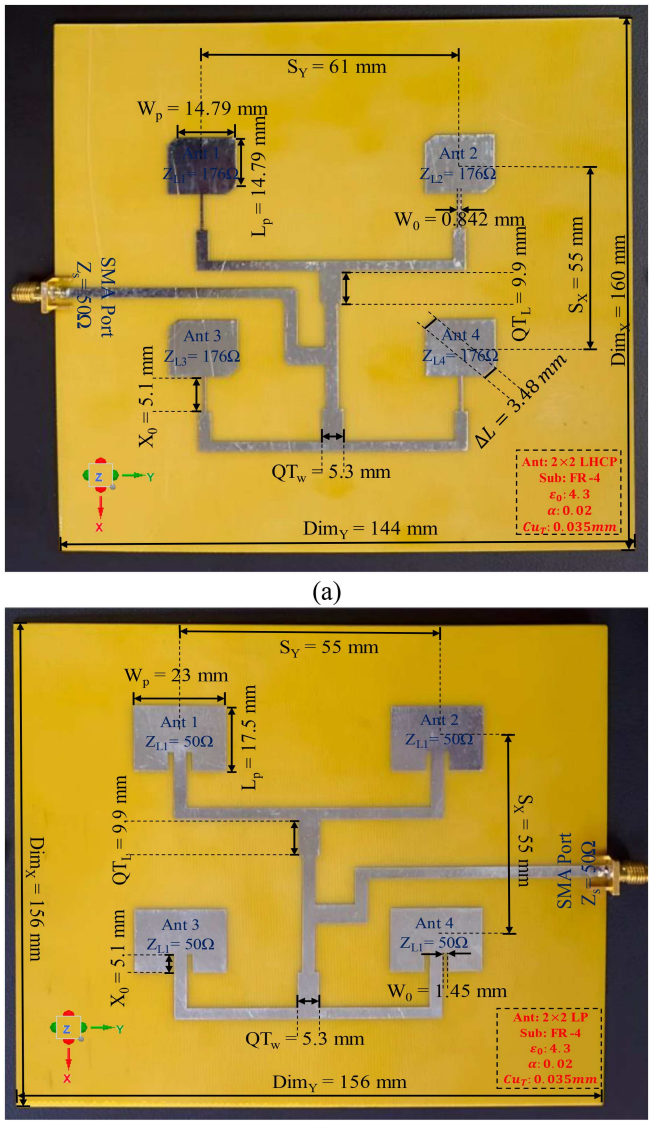

Fig. 8. Fabricated 4 GHz antenna array with four elements: (a) LHCP design with truncated corners and (b) standard LP design with inset fed array.

TABLE I
COMPARISON OF SIMULATED AND MEASUREMENT FOR 4 GHZ TX ANTENNA ARRAY

Parameter	Simulation	Measurement
S11 Return Loss (dB)	-13.65	-11.00
A.R.(dB)	0.70	0.85
Gain (dB)	7.22	7.17
Wave Pattern	LHCP	LHCP

analyze the measured A.R. and polarization wave pattern in Fig. 11(d).

Minor and major axes of the electric fields along the $X-Y$ plane in the far-field radiating region for both simulation and measurement results were determined in Fig. 11(d). Table I

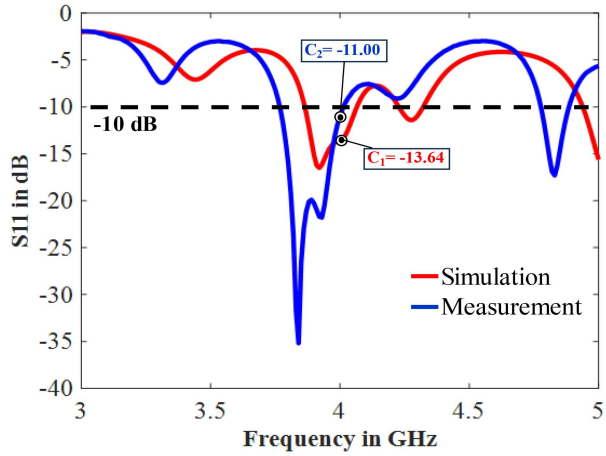

Fig. 9. Impedance matching for 4 GHz LHCP ant: simulation versus measurement in dB.

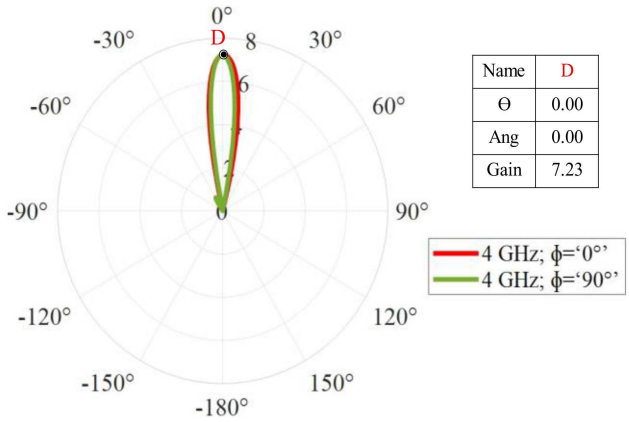

Fig. 10. 2-D simulation gain plot for 4 GHz LHCP ant in dB.

describes a comparison that summarizes the simulation and experimental information for the 4 GHz LHCP Tx array.

C. Rx Antenna: 8 GHz CP Antenna Array

The Rx antenna is primarily a CP four-element array designed for 8 GHz operating frequency for an LHCP array by incorporating the same approach of microstrip transmission feedline with 50 Ω input port excitation. LHCP array was designed based on a Rogers 3003 substrate ($\varepsilon_0 = 3.0$; $\alpha = 0.001$; $Cu_T = 0.035$ mm) for higher frequency applications. The array size dimensions were $94 \times 81 \times 0.25$ mm^3. The fabricated LHCP array is formed based on corner truncation ($\Delta L = 0.8$ mm) design as mentioned in Fig. 12(a) alongside other design marking considerations.

The standard 8 GHz fabricated LP array was designed primarily on gap inset fed ($X_0 = 3.22$ mm; $W_0 = 0.72$ mm) as shown in Fig. 12(b). The array elements spacing (S) distance is maintained in between $\lambda/2 < S\ in\ \text{mm} < \lambda$. Quarter wave transformers ($X_0 = 6.39$ mm; $W_0 = 0.2$ mm) were added to each element feeding edge for matching the load impedances ($Z_L = 176\,\Omega$) with the input source impedance ($Z_S = 50\,\Omega$). The

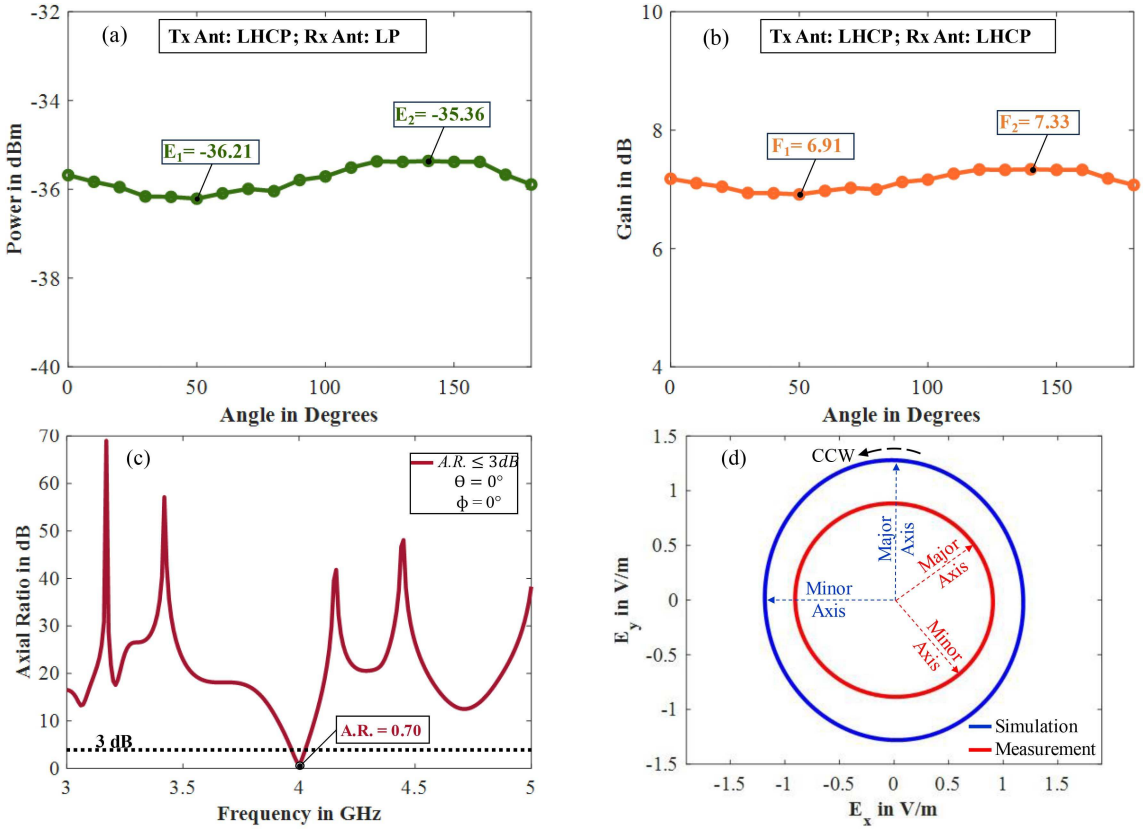

Fig. 11. (a) Measurement: angle versus received power signal plot, (b) measurement: angle versus gain plot, (c) simulation: A.R. versus frequency plot, and (d) polarization wave pattern: simulation versus measurement plots.

SMA connector of 0.6 mm gap clearance, which supports up to 26.5 GHz higher frequency broadband applications is soldered to the microstrip transmission feedline operating with the range of 7.6–8.2 GHz frequency span.

The three-equal power split technique was initially developed within the AWR microwave design environment with the primary objective of determining both the magnitude and phase data on the Smith chart.

The design parameters were replicated within the HFSS software to create a corporate feed network. This approach involves utilizing an SMA connector to transmit power through a transmission line. This line is then split into two equal segments using an initial $\lambda/4$ wave transformer. These divided power signals are then directed to supply energy to both the upper and lower halves of an array. These upper and lower sections of the array are connected in parallel and undergo another equal power division, this time facilitated by the second and third $\lambda/4$ wave transformers, respectively. At the junction of each $\lambda/4$ wave transformer, the widths of the microstrip feedlines are adjusted to align with the calculations for impedance matching.

The experimental setup is similar to 4 GHz LHCP measurement tests to determine the angle versus received power and angle versus gain plots. The setup consists of two sections. 1) 4 GHz LHCP Tx antenna mounted and rotated on a protractor platform by every 10° angle steps up to 360°; 2) 8 GHz LP Rx antenna is positioned on a fixed tripod stand facing opposite to the Tx antenna separated by 1.8 m in the far-field region to perform the polarization and gain estimation measurements. The received signal power is analyzed to understand the constant wave propagation with minimal signal distortion. The measurement data includes the maximum and minimum signal power in dBm. This information is essential in approximating the A.R. in dB. The gain estimation plot indicates the signal strength across the 10° angle steps. The polarization wave is also plotted on the of $|E_x|$ and $|E_y|$ along x- and y-axes, respectively.

The simulation and measurement validation of S_{11} return loss in Fig. 13 and simulated gain plot in Fig. 14. A.R. versus Frequency in dB plot in Fig. 15(c), and polarization wave pattern is shown in Fig. 15(d). The A.R. bandwidth for 8 GHz LHCP was ≤ 3 dB for both simulated and measured results. The accuracy of the A.R. simulation data points presented in Fig. 15(a) was confirmed through an additional step involving the extraction of simulated electric field vectors, along the x- and y-axes, respectively. Furthermore, the phase angles, denoted as $|E_x|$ and $|E_y|$, were simulated at angles $\angle\Theta = 0°$ and $\angle\phi = 0°$. This simulation is conducted to gain insights into the polarization orientation responsible for emitting a circular wave pattern in the far-field radiating region along the z-axis. The 8 GHz Rx array is designed to receive the reflected second-order harmonic tone from the tag. Table II presents a summarization of simulated and measured parameters for the 8 GHz LHCP array.

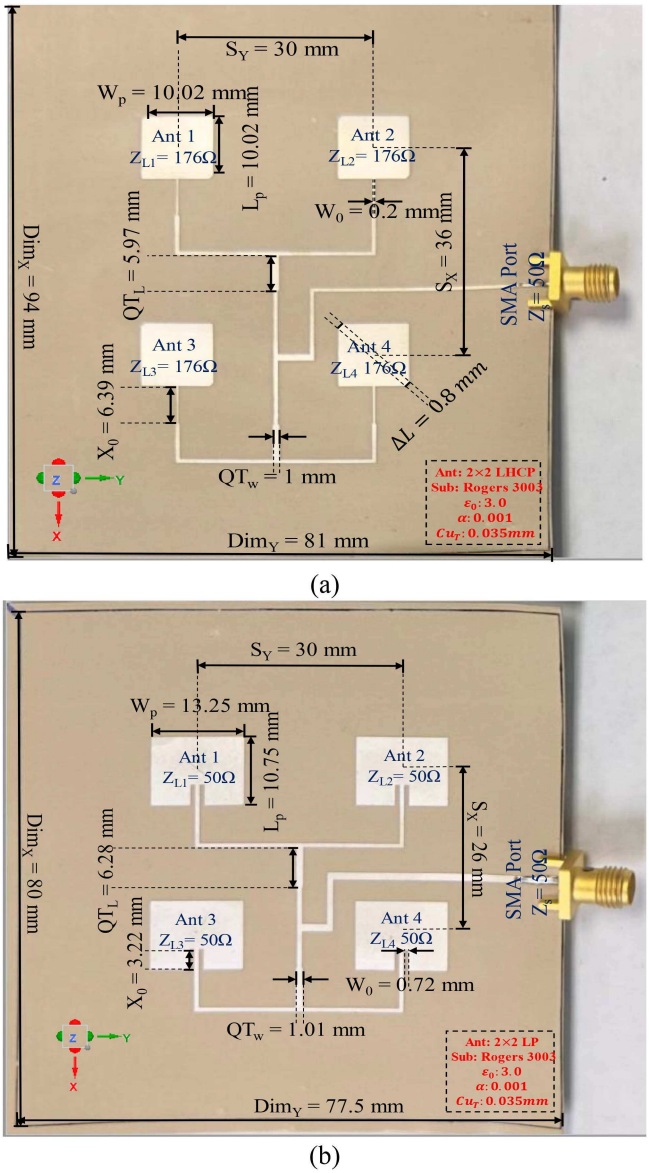

Fig. 12. Fabricated 8 GHz antenna array with four elements. (a) LHCP design with truncated corners. (b) Standard LP design with inset fed array.

TABLE II
COMPARISON OF SIMULATED AND MEASUREMENT FOR 8 GHZ TX ANTENNA ARRAY

Parameter	Simulation	Measurement
S11 Return Loss (dB)	-18.65	-14.20
A.R.(dB)	0.77	0.77
Gain (dB)	12.40	9.25
Wave Pattern	LHCP	LHCP

V. EXPERIMENTAL MEASUREMENTS AND RESULTS

To analyze the functionality of the snowflake tag detection and localization testing in the far-field radiating region [36], the experimentally verified LHCP Tx and the Rx radar antenna arrays discussed in Section IV, will be employed for performing

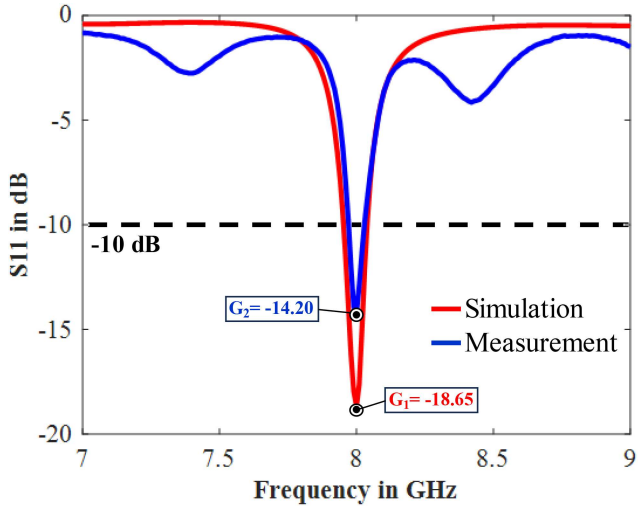

Fig. 13. Impedance matching for 8 GHz LHCP ant: simulation versus measurement in dB.

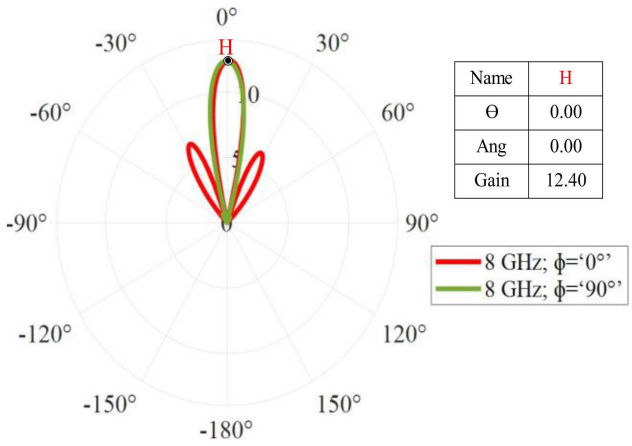

Fig. 14. 2-D simulation gain plot for 8 GHz LHCP ant in dB.

a novel harmonic snowflake tag tracking measurement discussed in [34] and [40]. The utilized snowflake antenna tag outperforms the conventional RFID antenna tags [37]. The fundamental block diagram of the test setup is shown in Fig. 16(a), and describes the working principle of tag detection and localization. The experimental measurement setup is depicted in Fig. 16(b). The measurement setup featured a Tx antenna positioned and rotated on a rotating polarization board/protractor marked at a 10° angle. This Tx antenna was paired with a stationary Rx antenna, positioned antennas were faced in the opposite direction of a snowflake tag, positioned at a distance of 0.40 m. in the far-field radiating region adjacently by a separation distance of 0.16 m. A semianechoic chamber with tapered RF absorbers setup is employed to enhance localization performance with minimal external signal interference.

The transmission setup includes a 4 GHz LHCP Tx antenna connected to a signal generator via a 50 Ω coaxial cable. The cable introduced a loss of 0.98 dBm. The experiment aimed to generate a constant signal peak, with the fundamental frequency

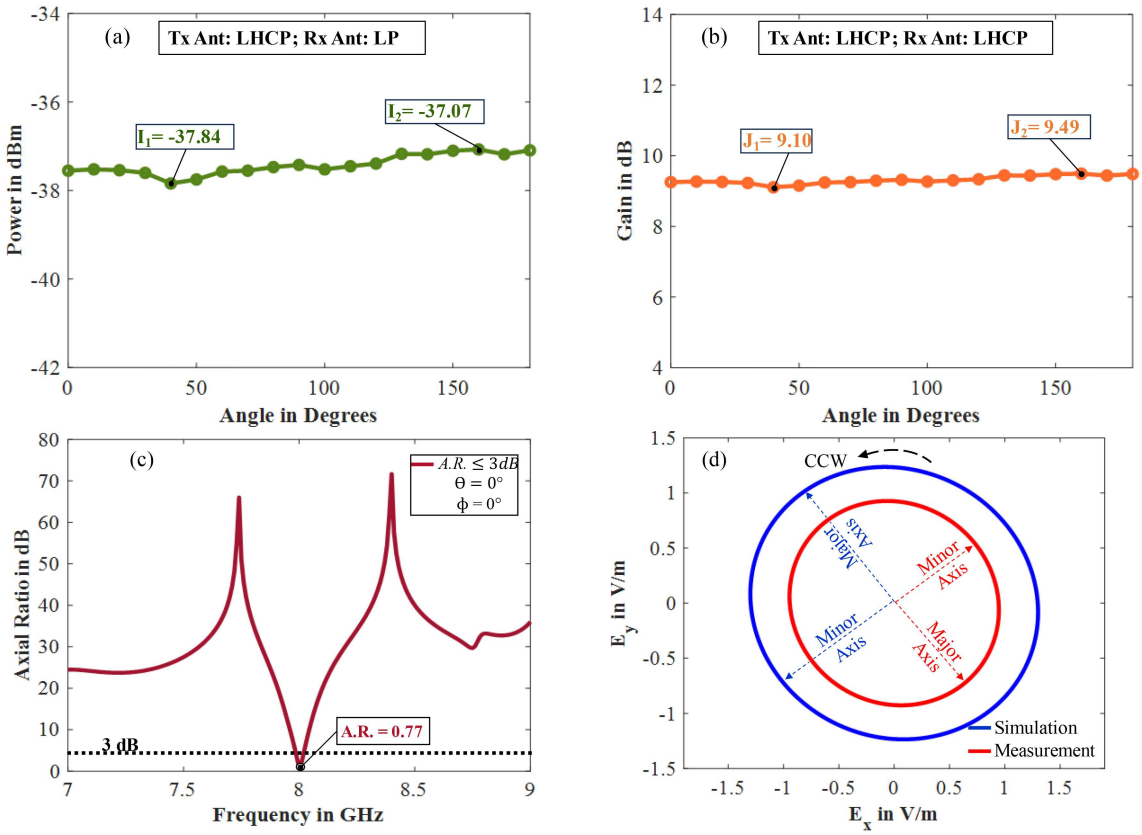

Fig. 15. (a) Measurement: angle versus received power signal plot, (b) measurement: angle versus gain plot, (c) simulation: A.R. versus frequency plot, and (d) polarization wave pattern: simulation versus measurement plots.

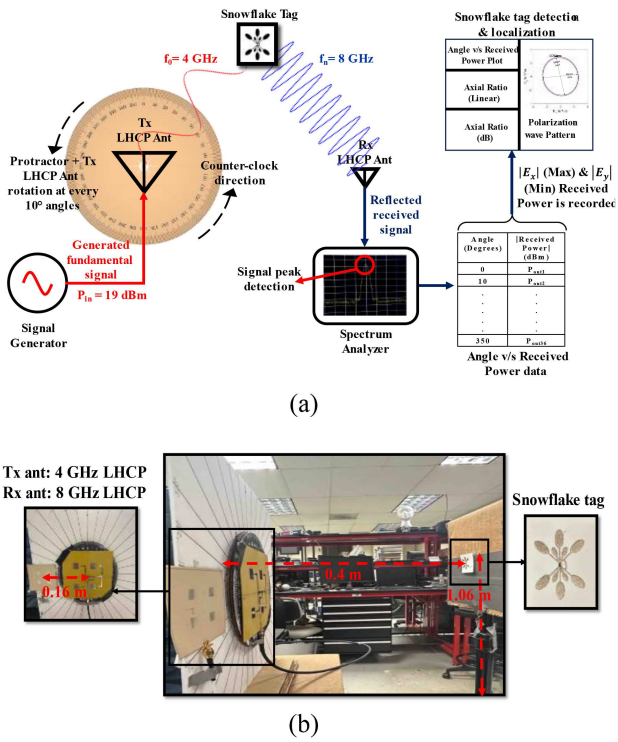

Fig. 16. (a) Block diagram and (b) experimental setup of snowflake tag detection and tracking with Tx: 4 GHz LHCP array and Rx: 8 GHz LHCP array.

sweeping from 3.8 to 4.2 GHz. The center frequencies were set at 3.9 GHz, due to the down-shifted frequency of the Tx CP antenna, with inputting a signal power (P_{in}) of 19 dBm. Interestingly, the CP design performed better at 3.9 GHz Tx signal.

A nonlinear snowflake passive tag is used as the target, that received the fundamental tone (4 GHz circular polarized wave). This passive snowflake tag reflected the fundamental frequency into a second-order harmonic frequency (8 GHz circular polarized wave). On the receiving end, the 8 GHz Rx antenna is connected to a spectrum analyzer using a 90° bend connector and a 50 Ω coaxial cable. The second-order harmonic frequency peak is detected in the range of 7.6–8.4 GHz, with center harmonic frequency marked at 7.8 GHz to match the fundamental tone range. The Rx cable introduced a loss of 3.07 dBm, and a stable continuous signal is observed at 7.8 GHz. Received signal power level data is recorded at 10° step intervals.

A graphical representation in Fig. 17. illustrates the relationship between angle (every 10° Tx antenna rotation) and received power level. The maximum received signal observed at 0° was −33.91 dBm. The minimum received signal observed at 60° was −36.81 dBm. The signal fluctuation or A.R. = 2.90 dB is achieved, which is mainly caused due to the snowflake tag bending, A.R. of the designed radar antennas, nonlinearities in tag and surrounding clutter noise. The received circular polarized wave pattern in Fig. 18. consists of the CCW wave rotation with major and minor axes. This verifies that the harmonic

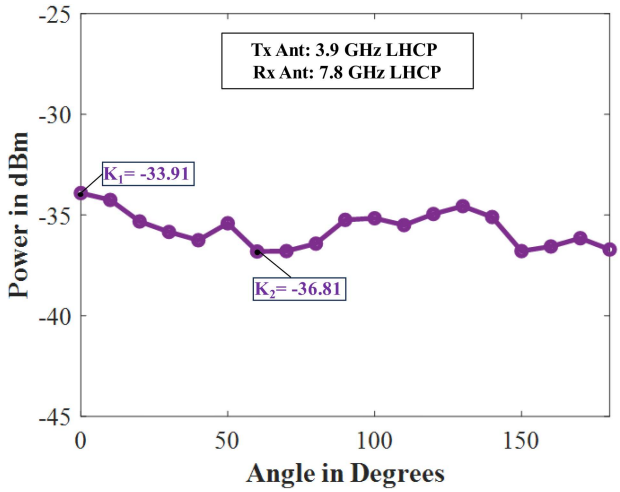

Fig. 17. Snowflake tag measurement for every 10° angle rotation of the Tx antenna.

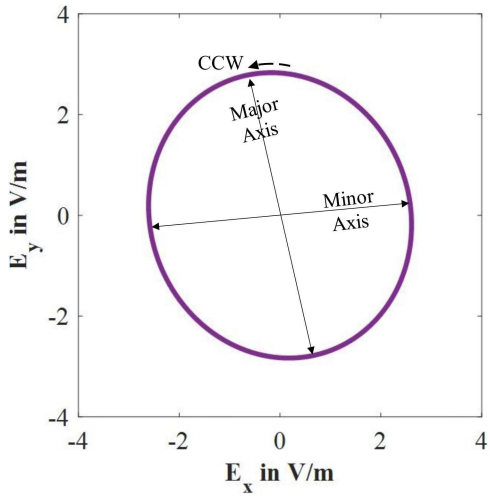

Fig. 18. Circular wave pattern for tag localization application.

TABLE III
TAG LOCALIZATION TEST MEASUREMENT

Parameter	Measurement
$\lvert E_Y \rvert_{(\mathrm{Min})}$ Angle (60°)	$\lvert -36.81 \rvert = 36.81$
$\lvert E_X \rvert_{(\mathrm{Max})}$ Angle (0°)	$\lvert -33.91 \rvert = 33.91$
A.R. (Linear)	-1.40
A.R. (dB)	2.90
Wave Pattern	LHCP

LHCP antennas were efficient in achieving a stable reflected return signal, which can be proved to detect and track the snowflake antenna tag. Table III summarizes the results of the tag detection and 2-D localization parameters, such as A.R. and $\lvert E_Y \rvert_{(\mathrm{Min})}$ and $\lvert E_X \rvert_{(\mathrm{Max})}$ angles. Fig. 17 verifies experimental results of the snowflake tag rotation with the maximum signal power at 0° angle and the minimum signal power at 60° angle. This theoretical and simulation results were supposed to be at 0° angle (maximum power) and 90° angle (minimum power). This would mainly occur due to the arrangement in the experimental setup/human error or fabrication error in the antenna arrays/nonlinear antenna tag.

VI. CONCLUSION

This research presents a novel snowflake tag detection and localization based on the principal methodology of harmonics. The snowflake tag design is implemented in HFSS software, to understand the conventional simulation results with a Schottky diode enabling a symmetrical dipole antenna tag with differential ports. The key design parameters, such as the current distribution and gain plot graphs, were improvised by visualizing that the snowflake tag performed better than the dipole antenna tag. The harmonic Tx and Rx LHCP antennas were designed at $f_0 =$ 4 GHz and $f_n =$ 8 GHz simulated, and the individual antenna performance is measured. Impedance matching S_{11} return loss, Gain estimation, A.R. (polarization measurement) and circular wave pattern were analyzed for tag tracking application. The novel snowflake tag detection and localization measurements were demonstrated to receive a stable continuous received signal with minimal signal fluctuation for rotating configuration of transmitting antenna. From this, we can analyze that since the transmitted and received waves are circularly polarized in nature facing the snowflake tag, if either of the Tx antenna, Rx antenna and the snowflake tag are rotated without changing its position orientation, the received signal power will be relative to each other with minimal signal degradation mentioned in [25]. Future work will include investigating the behavior characteristics of the snowflake tag with the complete demonstration of the portable harmonic radar system including the designed CP harmonic radar antenna arrays. This will result in a hand-held portable radar system applicable for tag localization of particular objects.

REFERENCES

[1] H. Stockman, "Communication by means of reflected power," *Proc. IRE*, vol. 36, no. 10, pp. 1196–1204, Oct. 1948.
[2] G. L. Charvat, E. J. Rothwell, and L. C. Kempel, "Harmonic radar tag measurement and characterization," in *Proc. IEEE Antennas Propag. Soc. Int. Symp.. Dig.. Held Conjunction: USNC/CNC/URSI North Amer. Radio Sci. Meeting*, 2003, vol. 2, pp. 696–699.
[3] R. Bansal, "Coming soon to a Wal-Mart near you," *IEEE Antennas Propag. Mag.*, vol. 45, no. 6, pp. 105–106, Dec. 2003, doi: 10.1109/MAP.2003.1282186.
[4] J. R. Riley et al., "Tracking bees with harmonic radar," *Nature*, vol. 379, pp. 29–30, 1996.
[5] H. Aumann, E. Kus, B. Cline, and N. W. Emanetoglu, "A low-cost harmonic radar for tracking very small tagged amphibians," in *Proc. IEEE Int. Instrum. Meas. Technol. Conf.*, 2013, pp. 234–237.
[6] T. T. Braun, J. Schopfel, C. Schweer, and N. Pohl, "A harmonic radar for bicycle detection with RFID tags at 79/158 GHz," in *Proc. IEEE/MTT-S Int. Microw. Symp.*, 2022, pp. 526–529.
[7] S. Bottigliero, D. Milanesio, M. Saccani, R. Maggiora, A. Viscardi, and M. M. Gallesi, "An innovative harmonic radar prototype for miniaturized lightweight passive tags tracking," in *Proc. IEEE Radar Conf.*, 2019, pp. 1–6.

[8] J. Huang, "A Ka-band circularly polarized high-gain microstrip array antenna," *IEEE Trans. Antennas Propag.*, vol. 43, no. 1, pp. 113–116, Jan. 1995.
[9] R. A. Lima, A. Mishra, and C. Li, "Advantages of utilizing higher-order response for a harmonic radar," in *Proc. IEEE Trop. Conf. Wireless Sensors Sensor Netw.*, 2022, pp. 29–31.
[10] H. Aumann, E. Kus, B. Cline, and N. W. Emanetoglu, "An asymmetrical dipole tag with optimum harmonic conversion efficiency," in *Proc. IEEE Int. Symp. Antennas Propag.*, 2012, pp. 1–2.
[11] F. Meloche and P. M. Albert, "A lighter transponder for harmonic radar," in *Proc. Eur. Radar Conf.*, 2007, pp. 233–236.
[12] M. Chao, Y. Guohui, K. Weidong, S. Shaorui, and W. Erchao, "Two kinds of miniaturized dual-band RFID planar antennas," in *Proc. Asia-Pacific Conf. Antennas Propag.*, 2014, pp. 558–561.
[13] H. J. Kim, S. M. Kim, J. M. Son, and W. G. Yang, "Design and implementation of dual band circular polarization square patch antenna," in *Proc. Asia-Pacific Microw. Conf.*, 2006, pp. 1–4.
[14] M. M. Khaleeq, A. W. M. Saadh, T. Ali, and B. S. Reddy, "A corner truncated circularly polarized antenna for IRNSS application," in *Proc. Int. Conf. Smart Technol. Smart Nation*, 2018, pp. 148–152.
[15] I. Radnovic, B. Jokanovic, and A. Boryssenko, "Circularly polarized patch antenna array at 24 GHz for radar applications," in *Proc. 26th Telecommun. Forum*, 2018, pp. 1–4.
[16] G. Li, H. Zhai, T. Li, L. Li, and C. Liang, "A compact antenna with broad bandwidth and quad-sense circular polarization," *IEEE Antennas Wireless Propag. Lett.*, vol. 11, pp. 791–794, Jul. 2012.
[17] M. S. Khan and F. A. Tahir, "A circularly polarized stacked patch antenna array for tracking applications in S-band," in *Proc. Eur. Conf. Antennas Propag.*, 2015, pp. 1–4.
[18] G. L. Lovei, I. A. N. Stringer, C. D. Devine, and M. Cartellieri, "Harmonic radar: A method using inexpensive tags to study invertebrate movement on land," *New Zealand J. Ecol.*, vol. 21, no. 2, pp. 187–193, 1997.
[19] K. A. Gallaghar, "Harmonic radar: Theory and applications to nonlinear target detection, tracking, imaging and classification," Ph.D. dissertation, Pennsylvania State Univ., University Park, PA, USA, Dec. 2015.
[20] G. J. Mazzaro, A. F. Martone, K. I. Ranney, and R. M. Narayanan, "Nonlinear radar for finding RF electronics: System design and recent advancements," *IEEE Trans. Microw. Theory Techn.*, vol. 65, no. 5, pp. 1716–1726, May 2017.
[21] G. J. Mazzaro, A. F. Martone, and D. M. McNamara, "Detection of RF electronics by multitone harmonic radar," *IEEE Trans. Aerosp. Electron. Syst.*, vol. 50, no. 1, pp. 477–490, Jan. 2014.
[22] K. A. Gallagher, R. M. Narayanan, G. J. Mazzaro, A. F. Martone, and K. D. Sherbondy, "Static and moving target imaging using harmonic radar," *Electronics*, vol. 6, no. 2, pp. 1–20, Apr. 2017.
[23] K. A. Gallagher, G. J. Mazzaro, A. F. Martone, K. D. Sherbondy, and R. M. Narayanan, "Derivation and validation of the nonlinear radar range equation," in *Proc. SPIE Conf. Radar Sensor Technol. XX*, 2016, vol. 9829, pp. 98290P-1–98290P-13.
[24] A. Abdelnour, A. Lazaro, R. Villarino, D. Kaddour, S. Tedjini, and D. Girbau, "Passive harmonic RFID system for buried assets localization," *Sensors*, vol. 18, no. 11, Oct. 2018, Art. no. 3635.
[25] G. J. Mazzaro et al., "Harmonic response vs. target orientation: A preliminary study of the effect of polarization on nonlinear junction detection," in *Proc. SPIE Conf. Radar Sensor Technol. XXVI*, 2022, pp. 1–21.
[26] K. A. Gallagher, R. M. Narayanan, G. J. Mazzaro, K. I. Ranney, A. F. Martone, and K. D. Sherbondy, "Moving target indication with non-linear radar," in *Proc. IEEE Radar Conf.*, 2015, pp. 1428–1433.
[27] M. B. Steer and P. J. Khan, "Large signal analysis of nonlinear microwave systems," in *Proc. IEEE MTT-S Int. Microw. Symp. Dig.*, 1984, pp. 402–403.
[28] B. Y. Toh, R. Cahill, and V. F. Fusco, "Understanding and measuring circular polarization," *IEEE Trans. Educ.*, vol. 46, no. 3, pp. 313–318, Aug. 2003.
[29] A. Chen, Y. Zhang, Z. Chen, and C. Yang, "Development of a ka-band wideband circularly polarized 64-element microstrip antenna array with double application of the sequential rotation feeding technique," *IEEE Antennas Wireless Propag. Lett.*, vol. 10, pp. 1270–1273, Nov. 2011.
[30] J. P. Daniel, G. Dubost, G. Terret, J. Citerne, and M. Drissi, "Research on planar antennas and arrays: 'Structures rayonnates'," *IEEE Antennas Propag. Mag.*, vol. 35, no. 1, pp. 14–38, Feb. 1993.
[31] I. J. Bahl and P. Bhartia, " Design considerations in microstrip antenna fabrication," in *Proc. Eur. Microw. Conf.*, 1980, pp. 122–126.
[32] S. Gao, Q. Luo, and F. Zhu, *Introduction to Circularly Polarized Antennas*. Hoboken, NJ, USA: Wiley, 2013, pp. 1–28.
[33] C. A. Balanis, *Antenna Theory: Analysis and Design*, 3rd ed. Hoboken, NJ, USA: Wiley, 2005.
[34] L. Zeng, D. Fazzini, R. B. Fazzini, S. W. Johnson, and C. Li, "Fast prototyping of nonlinear passive tags for location detection using harmonic radar," in *Proc. IEEE Radar Conf.*, 2023, pp. 1–4.
[35] X. Hui and E. C. Kan, "Radio ranging with ultrahigh resolution using a harmonic radio-frequency identification system," *Nature Electron.*, vol. 2, no. 3, pp. 125–131, Mar. 2019.
[36] Y. Ma, X. Hui, and E. C. Kan, "3D real-time indoor localization via broadband nonlinear backscatter in passive devices with centimeter precision," in *Proc. ACM Mobicom*, 2016, pp. 216–229.
[37] G. Marrocco, "The art of UHF RFID antenna design: Impedance-matching and size-reduction techniques," *IEEE Antennas Propag. Mag.*, vol. 50, no. 1, pp. 66–79, Feb. 2008.
[38] G. Storz and A. Lavrenko, "Compact low-cost FMCW harmonic radar for short range insect tracking," in *Proc. IEEE Int. Radar Conf.*, 2020, pp. 642–647.
[39] A. Lavrenko and J. Cavers, "Two-region model for harmonic radar transponders," *Electron. Lett.*, vol. 56, no. 16, pp. 835–838, Aug. 2020.
[40] V. G. Yadav, "Linear and circular polarization antenna array designs for harmonic radar system: Tag tracking application," M.S. thesis, Texas Tech Univ., Lubbock, TX, USA, Dec. 2023.

Vishal G Yadav (Graduate Student Member, IEEE) received the B.S. degree in electronics and communications engineering from Dayananda Sagar University, Bengaluru, India, in 2020. He joined Texas Tech University as an M.S. Research Assistant, where he worked on designing harmonic radar antenna arrays for 2-D non-linear passive tag localization in 2022. He received his M.S. degree in Electrical Engineering from Texas Tech University, Lubbock, TX, USA, in 2023.

He is currently working as an Electrical Engineer in R&D of RFID tracking system for the lab standards with Custom Calibration Solutions, LLC, Robbinsville, NJ, USA. His current research interests include radar antennas and their applications, antenna engineering, wireless sensing/tracking, microwave/RFID circuits and systems, and microwave/RF test equipment calibration.

Leya Zeng (Graduate Student Member, IEEE) received the B.S. and M.S. degrees in electrical engineering from the University of California at Riverside, Riverside, CA, USA, in 2020 and 2021, respectively. She is currently working toward the Ph.D. degree in electrical engineering with Texas Tech University, Lubbock, TX, USA.

His research interests include passive nonlinear tag and radar systems for wireless RF sensing, detection, signal processing, and their applications.

Changzhi Li (Senior Member, IEEE) received the B.S. degree in electrical engineering from Zhejiang University, Hangzhou, China, in 2004, and the Ph.D. degree in electrical engineering from the University of Florida, Gainesville, FL, USA, in 2009.

He is currently a Professor with Texas Tech University, Lubbock, TX, USA. His research interests include microwave/millimeter-wave sensing for healthcare, security, energy efficiency, structural monitoring, and human–machine interface.

Dr. Li is an IEEE Microwave Theory and Techniques Society (MTT-S) Distinguished Microwave Lecturer, in the Tatsuo Itoh class of 2022–2024. He was the recipient of the IEEE MTT-S Outstanding Young Engineer Award, the IEEE Sensors Council Early Career Technical Achievement Award, the ASEE Frederick Emmons Terman Award, the IEEE-HKN Outstanding Young Professional Award, and the NSF Faculty Early CAREER Award. He is an Associate Editor of IEEE JOURNAL OF ELECTROMAGNETICS, RF, AND MICROWAVES IN MEDICINE AND BIOLOGY.